Nanoscale observations of the epitaxial growth of hashemite on barite (001)

Alexander G. Shtukenberg [a,*], José M. Astilleros [b], Andrew Putnis [c]

[a] *Crystallography Department, St. Petersburg State University, Universitetskaya nab., 7/9, 199034 St. Petersburg, Russia*
[b] *Departamento de Cristalografía y Mineralogía, Facultad CC. Geológicas, Universidad Complutense de Madrid, Avda. Complutense s/n, 28040 Madrid, Spain*
[c] *Institut für Mineralogie, Universität Münster, Corrensstrasse 24. D-48149, Germany*

Abstract

The heteroepitaxial growth of hashemite $BaCrO_4$ on barite $BaSO_4(001)$ from supersaturated aqueous solutions was observed in situ using an atomic force microscope (AFM). It was shown that the first hashemite layer grows via two-dimensional nucleation easily forming a complete epitaxial layer, which is likely to have a low level of intrinsic stress. Two-dimensional nucleation of the second and subsequent layers proceeds with significantly lower rates, and growth occurs with lower step velocities. These layers seem to have significant level of intrinsic stress and tend to reduce it via the formation of free surface normal to the growth layer (holes in the layer, dendrite-like shape of nuclei and steps, preferable formation of nuclei at the step edges). As a result, the initially flat surface becomes rough. The process described corresponds to the Stranski-Krastanov epitaxial growth mode, which is well known for growth of semiconductor and metal films but not previously recognised for crystals grown from aqueous solutions.

Keywords: Atomic force microscopy; Solid–liquid interfaces; Surface structure, morphology, roughness, and topography; Crystallization; Epitaxy; Growth; Nucleation

1. Introduction

Heteroepitaxial structures are widely used for fabrication of various electronic devices and, for this reason, their formation is widely studied both theoretically and experimentally [1]. Consequently, most of these researches are restricted to a narrow

* Corresponding author. Tel.: +7 812 3289647; fax: +7 812 3284418.
E-mail address: sasha@as3607.spb.edu (A.G. Shtukenberg).

class of semiconductors, metals and oxides grown mainly by the method of molecular beam epitaxy [2,3]. Studies of epitaxial structures produced during crystal growth from aqueous solution are more scarce and data on the nanoscale epitaxial processes are still lacking. However, epitaxial growth from aqueous solutions is a very usual phenomenon commonly observed both in nature and laboratory. An especially extensive phenomenon is the formation of solid solutions grown from aqueous solutions, since many minerals and synthetic compounds form solid solutions with complicated zoning patterns. Compositional and oscillatory zoning can be considered as heteroepitaxy, because it suggests a growth on the substrate with very similar crystal structure but different chemical composition and lattice constants. Therefore, understanding heteroepitaxial processes in solid solution–aqueous solution systems (SS–AS) is relevant in the study of zoning and related phenomena in natural and synthetic crystals.

A strong effect of substrate on a growth layer of different composition (template effect) has been reported in [4,5] for several heteroepitaxial systems. It was shown that the step velocity, significant for the first epitaxial layer, is reduced drastically for subsequent layers approaching a zero value.

In this paper we continue the study of heteroepitaxial growth in SS–AS systems, but only focusing on the processes taking place during the growth of one end-member directly on the other one. As a model system we have chosen the growth of hashemite ($BaCrO_4$) on barite ($BaSO_4$) (001) substrate. These compounds form a complete and ideal solid solution [6] crystallizing in the orthorhombic space group *Pnma*. They have the similar lattice constants: $a = 8.878$ Å, $b = 5.450$ Å and $c = 7.152$ Å for barite [7] and $a = 9.105$ Å, $b = 5.541$ Å and $c = 7.343$ Å for hashemite [8]. Because of their similarity in solubility products ($K_{sp,hashemite}/K_{sp,barite} = 2.04$) and lattice constants, this system is suitable to study epitaxial growth taking place in SS–AS systems. Epitaxial growth experiments were made in a fluid cell of a Digital Instruments Multimode AFM working in contact mode.

2. Experimental

Experiments were carried out at 25 °C in situ in a fluid cell of a Digital Instruments Multimode AFM. Due to the strong adhesion of the growing layers in the substrate, AFM worked in contact mode. AFM images were usually taken by scanning a conical Si_3N_4 tips (spring constant 0.12 N/m) attached to a 200 m cantilever (Digital Instruments). Sometimes shorter tips (100 μm) with spring constant 0.48 N/m were used. Height images were improved (flatten) using the NanoScope software (Version 5.12b48). Freshly cleaved, optically clear (001) barite surfaces were used as substrates. Hashemite was crystallized from solutions prepared by mixing of $BaCl_2$ and Na_2CrO_4 aqueous solutions. Before each growth experiment, deionised water was passed over the crystal to clean the cleaved surface, as well as to adjust the AFM parameters.

For barite on barite crystallization Na_2SO_4 solutions were used instead of Na_2CrO_4 solutions. Activities of different chemical species with respect to hashemite and barite were calculated using

Table 1
Concentrations and supersaturations with respect to hashemite of the solutions used in the AFM experiments

Experiment number	Solution composition				Supersaturation $\ln\beta$
	$BaCl_2$ (mmol/l)	Na_2CrO_4 (mmol/l)	a (Ba^{2+})	a (CrO_4^{2-})	
1	0.032	0.032	3.2×10^{-5}	1.1×10^{-5}	0.345
2	0.039	0.039	3.6×10^{-5}	1.5×10^{-5}	0.944
3	0.043	0.043	4.0×10^{-5}	1.8×10^{-5}	1.221
4	0.053	0.053	5.3×10^{-5}	2.8×10^{-5}	1.773
5	0.062	0.062	5.7×10^{-5}	3.3×10^{-5}	2.164
6	0.065	0.065	6.0×10^{-5}	3.5×10^{-5}	2.279

PHREEQC [9]. Supersaturation was calculated as $\ln \beta = \ln(\prod_i a_i / K_{sp})$, where a_i is the ion activity ($i = Ba^{2+}$, CrO_4^{2-} or SO_4^{2-}), K_{sp} is the solubility product (equal to $10^{-9.67}$ and $10^{-9.98}$ for hashemite and barite, respectively [10,11]). Concentrations of the solutions used in experiments and calculated supersaturations with respect to hashemite are listed in Table 1. To avoid solution/sample equilibrium a flow of solution was maintained by injecting fresh solution at intervals of about 1 min between each AFM scan. The step velocities as well as the nucleation rates were measured from time sequences of AFM images.

3. Results

Once barite (001) surfaces were cleaned and the AFM parameters adjusted, solutions supersaturated with respect to hashemite were injected in the fluid cell. Since the Na_2CrO_4 and $BaCl_2$ solutions are free from the sulfate ions and barite substrate dissolves negligibly during our experiments the SO_4^{2-} concentration at the crystal/solution interface and in the precipitate has to be negligible and the new deposited layers can be considered as pure hashemite. As can be expected, the growth behavior strongly depends on the supersaturation.

At low supersaturation ($\ln \beta < 0.8$) the growth only occurs via tangential motion of existing cleavage steps. As in the case of barite growing on barite, the cleavage steps of one unit cell height ($c = 7.15$ Å) split into two elementary growth steps ($h = 3.67$ Å) which have very strong growth anisotropy, so that the fast growing steps move about 10 times faster than the slow ones [12,13]. The fastest (and slowest) growth directions have the opposite orientations in the adjacent layers which are symmetrically related by a 2_1 screw axis.

At higher supersaturations ($\ln \beta > 0.8$) two-dimensional nucleation begins to contribute significantly to the growth of the first epitaxial layer. The growth of this layer seems to proceed in a very similar way to barite on barite (001) homoepitaxial growth [12,13]—a representative example is shown in Fig. 1a (supersaturation with respect to hashemite is $\ln = 1.773$). The nuclei have the sector-like shape, which is very close to that observed for barite [12,13], however, the angle at the apex of the sector for hashemite is ~60° in comparison with ~100° for barite. In our case, the straight steps of the hashemite nuclei are, therefore, parallel to a PBC (periodic bond chain) different from ⟨120⟩ (which define the orientation of the barite nuclei steps [12,13]) the ⟨110⟩ PBC being the best candidate. For the considered case (Fig. 1) the barite surface was completely covered by this first hashemite layer after 7 min.

At relatively low supersaturation ($\ln \beta < 1.5$) no nucleation on the first deposited layer is visible and growth nearly stops after completion of the first layer. At higher supersaturation ($\ln \beta \approx 1.8$) nucleation on the first hashemite layer takes place. However, the growth of the second and following epitaxial layers differs drastically from the growth of the first one. In contrast to the first layer, where the nuclei are randomly distributed over the crystal surface, nuclei of the second layer grow on preferential areas, specifically, step edges. Fig. 1b–d (supersaturation $\ln \beta = 1.773$) and Fig. 2 (supersaturation $\ln \beta = 2.164$) clearly show that the new layers are more easily formed on the top of the nuclei and areas already covered by two or more epitaxial layers. At a given relationship between nucleation rates and step velocity new 'on-top' layers nucleate faster then the previous layers are completed and the crystal surface becomes rough. The shape of nuclei changes as well. At supersaturation $\ln \beta = 1.773$ the nuclei have irregular and sometimes even dendrite-like shape and contain numerous pores (Fig. 1). The same porous or dendritic structure characterizes the advancement of existing steps (e.g., A and B in Fig. 1c). At higher supersaturation ($\ln \beta > 2$) nucleation proceeds more easily and the nucleus shape is closer to the usual sector-like shape (Fig. 2). Nucleation at these special sites proceeds ~2–40 times slower than nucleation of the first layer on the barite substrate, whereas nucleation on the flat surface covered by one hashemite layer is ~90–400 times slower than nucleation on the barite substrate (Fig. 3).

Growth of the second and subsequent epitaxial layers is accompanied by lower velocity compared

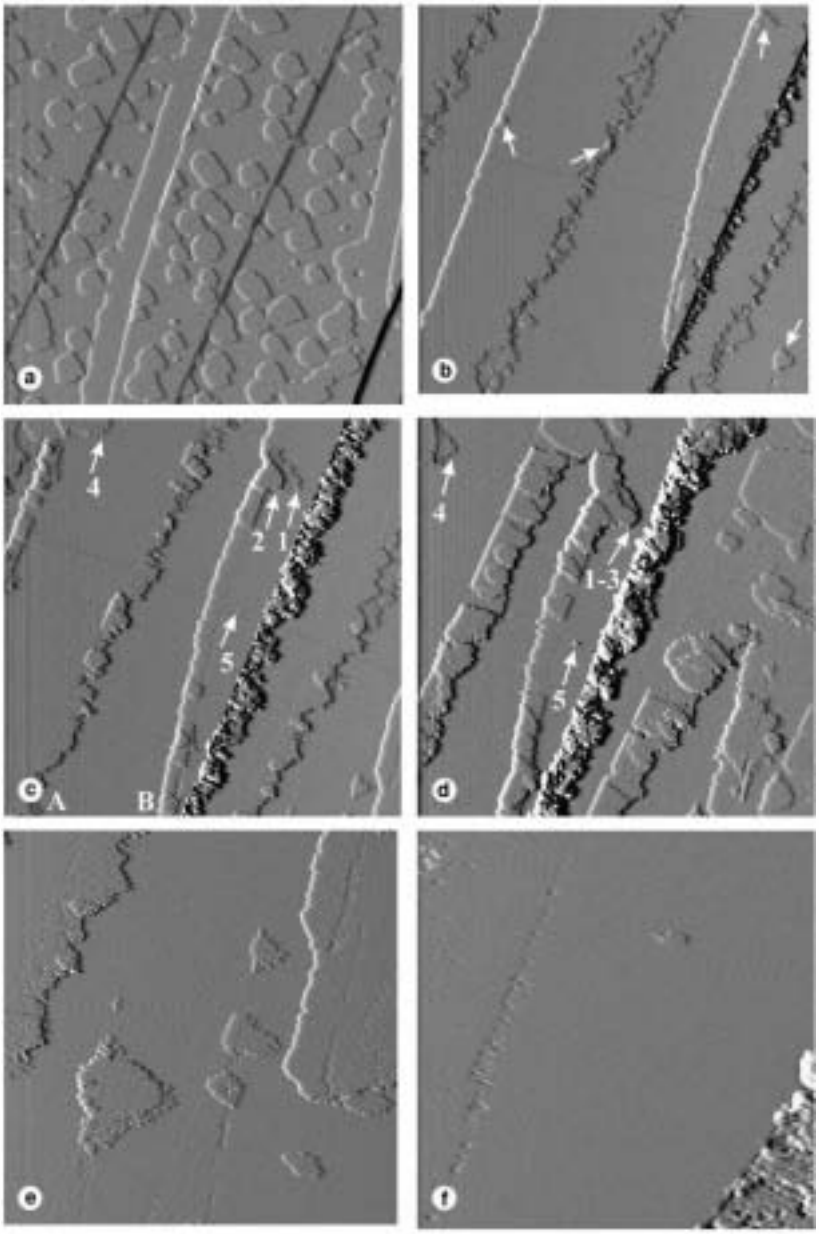

Fig. 1. Growth of $BaCrO_4$ on $BaSO_4$(001) substrate, supersaturation $\ln\beta = 1.773$. (a) 12.5 min after injecting the growth solution, numerous sector-shaped nuclei cover almost all the substrate. Original cleavage steps split into two steps growing with very different velocities. The thick black line at the lower right is a step of large height. (b) After 25.5 min the substrate is fully covered by a first hashemite layer and the growth of the second layer starts (arrows mark the first nuclei on the hashemite layer). (c) After 41 min a significant number of nuclei was formed, appearing most of them near the step edges and on the areas covered by few hashemite layers. The high step produces irregular and very complicated growth forms. (d) After 68.5 min the surface becomes substantially rough. Most of growth islands are located in the regions covered by few hashemite layers and do not extend beyond the boundaries of these areas. The area of images (a) (d) is 7 μm × 7 μm. (e) The nuclei and growth steps growing on the hashemite layer have irregular shape with numerous pores, the area of image is 3 μm × 3 μm. (f) Detailed image of the nucleus marked in Fig. 1c and d by number 5, the area of image is 1 μm × 1 μm.

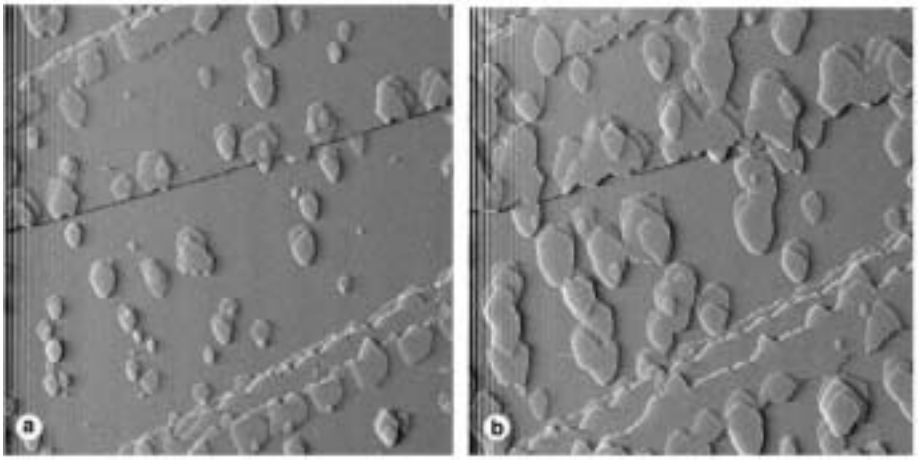

Fig. 2. Growth of $BaCrO_4$ on $BaSO_4$(001) substrate, supersaturation $\ln\beta = 2.164$. The images, taken (a) after 30 min after injecting the solution and (b) after 42 min show the evolution of the surface covered by one hashemite layer. Most nuclei are formed on the top of preexisting nuclei and close to their edges. The area of both images is 15 μm × 15 μm.

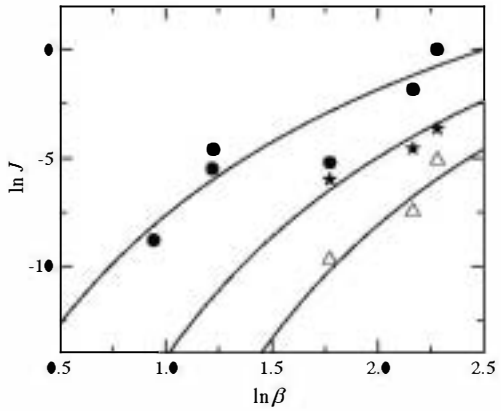

Fig. 3. Effect of supersaturation on the nucleation rate (J in $\mu m^{-2}\ s^{-1}$) for the first (circles), second (triangles) and third + fourth (stars) hashemite layer on the barite (001) substrate. The lines were calculated with Eq. (3), $\ln C = 12$, $K_2 = 51.1$.

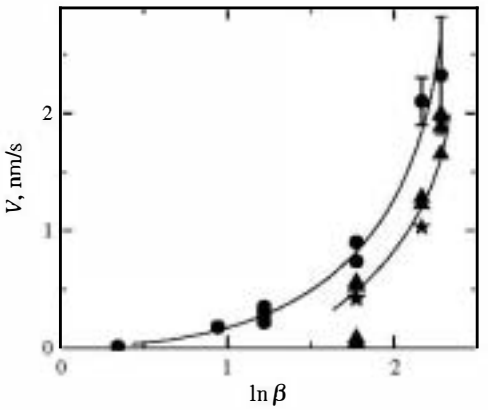

Fig. 4. Step velocity of the first (circles), second (triangles) and third + fourth (stars) hashemite layer on barite (001) substrate. Lines are guides for eyes.

with the first layer, however, the growth velocity is not a constant for different nuclei and even for the same nucleus (Fig. 4). Starting from the second layer each following layer seems to grow slightly more slowly than the previous one (Fig. 4). In contrast to barite and to the first hashemite layer the anisotropic growth of the second and subsequent hashemite layers diminishes significantly and the fastest to slowest velocity ratio does not exceed the factor of two (compare e.g., steps A and B in Fig. 1c).

4. Discussion

4.1. Growth velocity

Fig. 5 shows the growth velocity in the fastest direction V as a function of supersaturation for the first epitaxial layer of barite and hashemite on barite (001) substrate. In the last case, the experimental points deviate significantly from the linear function shown for the homoepitaxial growth of many compounds (e.g., for $NaClO_3$ and $NaNO_3$ [14]) and predicted by theory and

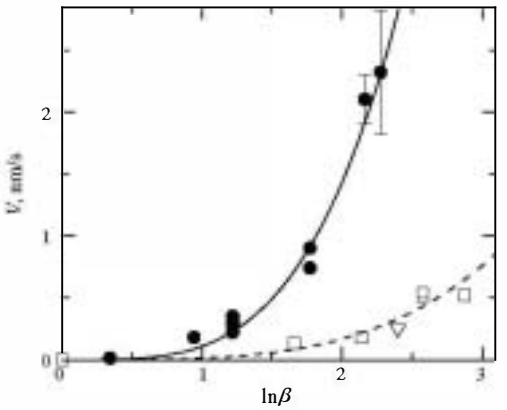

Fig. 5. Step velocity the fastest direction as a function of supersaturation for first layer of hashemite (solid symbols) and barite (open symbols) on barite (001) substrate, circles and squares our data, triangle data from [12]. The error bars if not shown are within the symbol sizes. Lines are fits with a power function.

can be rather approximated by a power function $V = \xi(\ln\beta)^{3.7}$, with the kinetic coefficient $\xi = 0.11$ nm/s for hashemite. At this moment we do not have a reliable explanation of this non-linearity, because, unfortunately, there are neither previous data nor a well-developed theory concerning the step advancement velocities of heteroepitaxial layers. For homoepitaxial growth of some other compounds a similar behaviour is explained through action of impurities, which adsorb on the crystal face and reduce the step propagation [15,16]. Our data suggest that the substrate can exert an important role in the steps advancement kinetics.

4.2. Heteroepitaxy vs. homoepitaxy

Compared with the homoepitaxial growth, heteroepitaxy is affected by at least two additional factors. The first is the elastic stress. The formation of the interface between two layers requires matching of their lattice planes (Fig. 6a). If the difference between the corresponding lattice constants is not too high, the lattice matching results in the formation of a coherent substrate–film interface and the generation of elastic strain and stress. The elastic stress and the associated elastic energy U_{max} are concentrated only in the epitaxial layer and distributed uniformly over the epitaxial film as long as its overall thickness is significantly lower than the lateral size and the thickness of the substrate (so-called pseudomorphic epitaxial growth, Fig. 6b) [3].

Since the elastic energy increases the free energy of the film, the stress relaxation starts. Misfit dislocations are unlikely to appear in such thin layers (2 unit cells or lower), so the *free surface* relaxation mechanisms are expected to be predominant.

For the first (1 up to 5) epitaxial layers it is possible to minimize the elastic energy via independent normal and lateral displacements of atoms (Fig. 6c). This possibility is not taken into account by the classical theory of elasticity, which considers the layer as a continuous medium and does not deal with the atomic arrangement. Thus the surface layer has a low level of intrinsic stress but it becomes crimped and complicated by additional displacements of atoms. In the first layer, such displacements should be most pronounced and can reduce the elastic energy significantly (down to the value of $U < U_{max}$). As successive hashemite layers grown on the substrate, these displacements become inconsistent with the volume crystal structure of the growing layer (Fig. 6d) and vanish progressively. This leads to elastic energy storage and achievement of U_{max} value.

Another way to reduce the misfit energy consists in the formation of additional free surface normal to the growth layer. The presence of such a surface allows free displacements of atoms in direction parallel to the growth layer and, in accordance with St. Venant's principle, it leads to a decrease of the stress near to the free surfaces at distances of about a growth layer in height. Thus the rough surface results in a reduction of elastic energy but an increase in surface energy. If the elastic energy decrease is greater than the surface energy increase the flat surface becomes unstable and can becomes rough (the so-called Grinfeld instability, see e.g., [17–19]).

The second factor is the difference in interfacial surface energies between the epitaxial film γ_f and substrate γ_s and the appearance of additional specific interface free energy γ_{fs} [2,3]. At certain relationships between these values the epitaxial layer can either easily form a complete layer

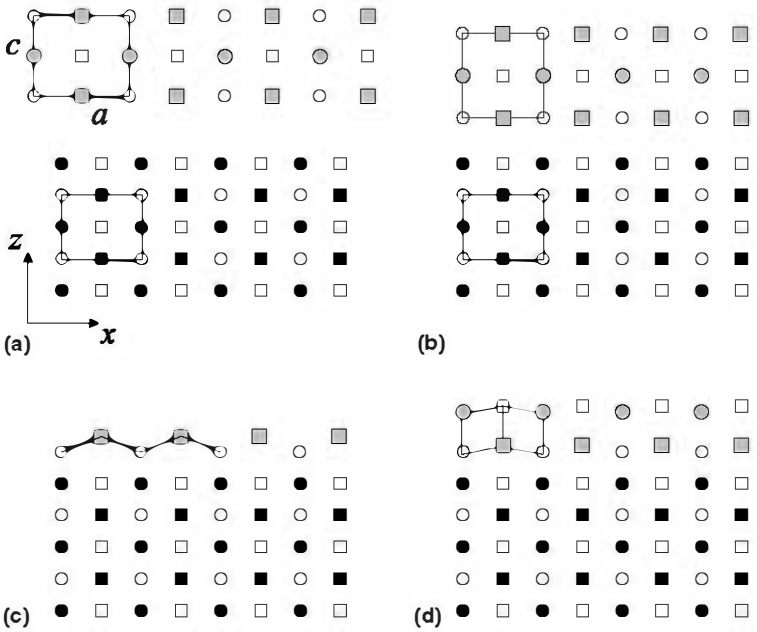

Fig. 6. Schematic representation of the surface relaxation mechanism. Open symbols cations Ba^{2+}, black symbols anions SO_4^{2-}, grey symbols anions CrO_4^{2-}, circles $y = b/4$, squares $y = 3b/4$. (a) Barite substrate (below) and hashemite layer (above). (b) Ideal pseudomorphic growth of hashemite on barite, the hashemite layer is under strong compressive strain and stress. (c) Surface relaxation of the single hashemite growth layer on the barite substrate. The bonds lengths Ba^{2+} SO_4^{2-} and Ba^{2+} CrO_4^{2-} have the typical values for barite and hashemite, respectively. Displacements of atoms are high, but stress is absent. (d) Deposition of two hashemite layers reduces the surface relaxation, since the atomic displacements are inconsistent with the hashemite crystal structure. The atoms move to their ideal positions and stress appears. After deposition of few layers the usual pseudomorphic growth can be observed.

(Frank–Van der Merwe growth mode) or tend to form three-dimensional islands on the substrate surface (Volmer–Weber growth mode). Elastic strain can also affect the surface and interface energies [2,3] so these two factors should be considered together.

4.3. Qualitative interpretation of results

The ideas formulated above give us a basis for explanation of the phenomena observed. The easy growth of the first hashemite layer is possible due to the surface relaxation of misfit stress (Fig. 6) and the close values of the surface energies ($\gamma_f \approx \gamma_s$, see below). The growth of the second and following epitaxial layers should be accompanied by a higher level of intrinsic stress, since the surface relaxation becomes less effective.

Increasing of the free energy of the layer decreases the driving force of crystallization that reduces the nucleation rate (Fig. 3). In particular, it leads to preferred formation of 2D nuclei at edges of steps and on the areas already covered by two or more hashemite layers. Easy nucleation near to the step edges results from the lower level of stress near to additional free areas. However, easy nucleation on the areas covered by few hashemite layers looks surprising since such a process should lead to lower degree of the surface relaxation and to higher level of stress. We believe that preferable nucleation at these sites results from very high imperfections of such areas. Fig. 1e shows numerous holes in the second epitaxial layer which can decrease the stress and facilitate the nucleation. The chains of holes allow even to visualize the regions covered by two or more epitaxial layers (Fig. 1e and f). Significant imperfections of deposited layers can be seen from dissolution experiments, where replacement of supersaturated hashemite solution by clear water induced the fast and complete dissolution of the deposited layer (Fig. 7). Since dissolution starts not only from

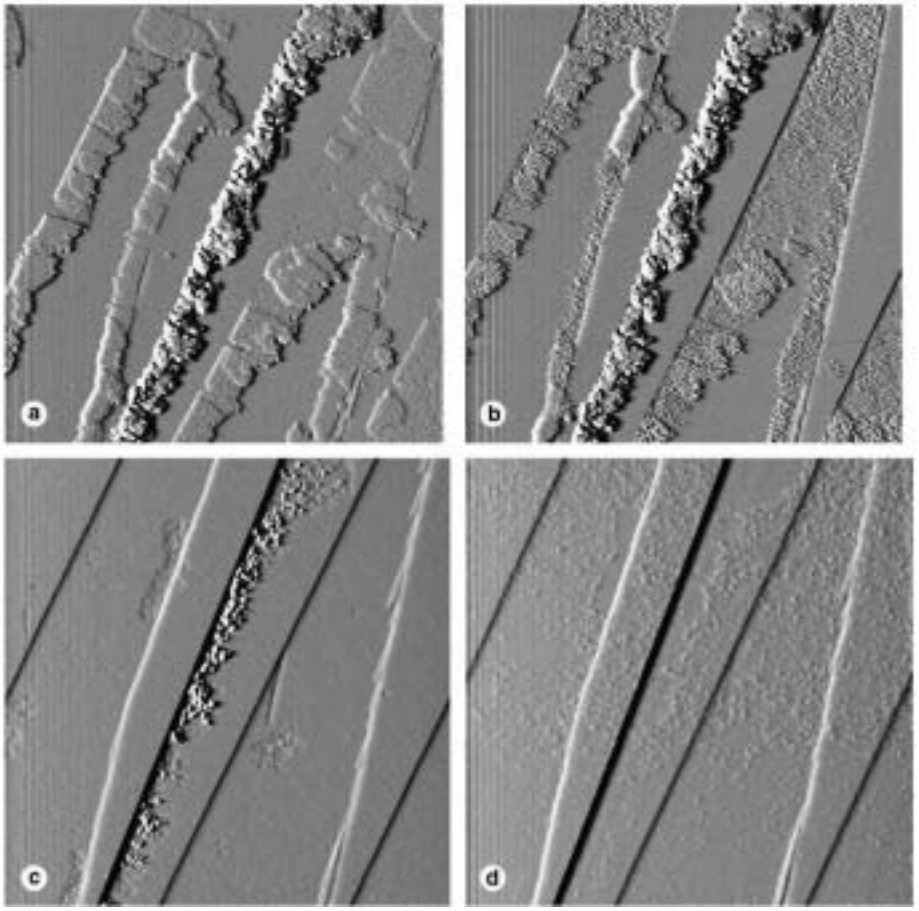

Fig. 7. Dissolution patterns of the crystal shown in Fig. 1d. Images a and b were recorded in 1.5 min and 8.5 min after injecting the saturated hashemite solution, respectively. All the deposited hashemite layers, with exception of the first one, are dissolved. Replacement of hashemite solution by clear water induces dissolution of the first hashemite layer. Images c and d were recorded in 4.5 min and 6.5 min after injecting deionised water and show the initial stages of dissolution and nearly complete removing of the first hashemite layer, respectively. The area of the images is 7 μm × 7 μm.

the step edges but also from the numerous etch pits distributed uniformly over the crystal surface, it would be reasonable to suggest that the epitaxial layers contain numerous very small (invisible) holes, which act as dissolution centers. At higher supersaturations, the second and following layers look more perfect and nucleation takes place preferably at step edges or at boundaries between the regions covered by one and few (usually by three) hashemite layers (Fig. 2). On the one hand, these boundaries facilitate nucleation behaving like a surface defect. On the other hand, they stop or, at least, slow down the growth of nuclei in corresponding directions (Figs. 1 and 2). Such a behaviour can be explained by the presence of an additional energetic barrier there. At this boundary, the crystal surface forms a step of about $c_{\text{hashemite}} - c_{\text{barite}} \approx 0.19$ Å (c is a lattice constant [7,8]), which hinders the growth step propagation. The presence of such a surface step can be seen in Fig. 2 (see also data on some solid solution–aqueous solution systems [20]).

Increasing of the free energy of the layer also results in a decrease of the step velocity (Fig. 4). The high scatter of measured values can be associated with the surface imperfections i.e., with the local

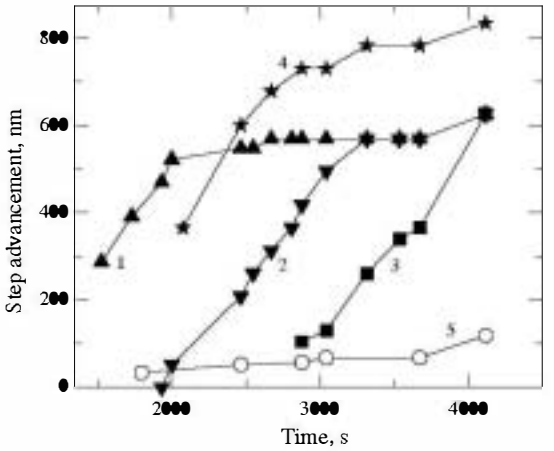

Fig. 8. Step advancement for few nuclei (numbers near the lines correspond to nuclei marked in Fig. 1c and d) as a function of time.

stress. For instance, the nuclei formed on the flat surface covered by one hashemite layer grow very slowly (see nucleus 5 in Figs. 1c, d, f, and 8) compared with the nuclei formed near to the step edges on the surface covered by few hashemite layers (see nuclei 1–4 in Figs. 1c, d and 8). However, the growth velocity of these "successful" nuclei can be reduced significantly when they reach some points on the crystal surface (Fig. 8), where the stress is probably higher.

The different level of stress between the first and the following layers can be clearly seen from the dissolution experiment, where all the deposited hashemite layers, with the exception of the first one, were completely dissolved by a *saturated* solution of $BaCrO_4$ (Fig. 7a and b). Thus, in contrast to the first epitaxial layer, the second and subsequent layers have significant level of intrinsic stress and tend to reduce it via formation of free surface normal to the growth layer (holes in layer, dendrite-like shape of nuclei and steps, preferable formation of nuclei at the step edges).

It is worth noting that the different structural state of the first and the following epitaxial layers can be seen from the growth anisotropy. The first layer inherits the growth anisotropy of the substrate (Fig. 1a), whereas the following layers have significantly lower degree of anisotropy (Figs. 1c, d and 2), see also [21].

4.4. Calculation of misfit energy

Let us assume a thin hashemite layer grown on the thick (001) barite substrate. Barite and hashemite belong to the orthorhombic system so that the strain tensor in the interface plane has two non-zero components: $\varepsilon_1 = (a_{\text{hashemite}} - a_{\text{barite}})/a_{\text{barite}} \approx 0.026$ and $\varepsilon_2 = (b_{\text{hashemite}} - b_{\text{barite}})/b_{\text{barite}} \approx 0.017$, where a and b are lattice constants [7,8]. The third non-zero component of the strain tensor follows from the Hooke law and the zero stress normal to the interface $\sigma_3 = c_{13}\varepsilon_1 + c_{23}\varepsilon_2 + c_{33}\varepsilon_3 = 0$, where c_{ij}—elastic stiffness constants. Since the stress tensor has two non-zero components $\sigma_1 = c_{11}\varepsilon_1 + c_{12}\varepsilon_2 + c_{13}\varepsilon_3$ and $\sigma_2 = c_{12}\varepsilon_1 + c_{22}\varepsilon_2 + c_{23}\varepsilon_3$, the elastic energy of the layer is written as

$$U_{\max} = \frac{w}{2}\sum_{i=1}^{6}\sigma_i\varepsilon_i = \frac{w}{2}\left[\varepsilon_1^2\left(c_{11} - \frac{c_{13}^2}{c_{33}}\right) + 2\varepsilon_1\varepsilon_2 \times \left(c_{12} - \frac{c_{13}c_{23}}{c_{33}}\right) + \varepsilon_2^2\left(c_{22} - \frac{c_{23}^2}{c_{33}}\right)\right], \quad (1)$$

where $w = 9.26 \times 10^{-29}$ m^3 denotes molecular volume of hashemite. Unfortunately, we did not find values of the elastic constants for hashemite and we have used the values for barite [22]. Substitution of numerical values finally gives $U_{\max} = 5.24 \times 10^{-21}$ J or $U_{\max}/kT = 1.275$, where $k = 1.38 \times 10^{-23}$ J/K is the Boltzmann constant and T is the absolute temperature.

4.5. Driving force of crystallization

The driving force of crystallization is defined by the difference between the chemical potentials in solution and in the crystal $\Delta\mu_0 = kT\ln\beta$. The elastic stress energy increases the chemical potential and solubility of the crystal and, hence, reduces the driving force down to the value $\Delta\mu = \Delta\mu_0 - U_{\max}$. This simple correction can provide some interesting phenomena. For example, the step intersecting two parts of the crystal face with different level of intrinsic stress will grow with different velocities. At certain conditions it is possible to get the simultaneous growth of one part of the step and dissolution of another part, as was observed for sodium chlorate crystals [14]. At the macroscale, simulta-

neous growth of one face and dissolution of the adjacent face was observed for the zonal potassium–rubidium biphthalate crystals [23,24].

A more accurate approach includes the surface and interface energies, since attachment of a growth unit to a crystal surface creates a new surface with the energy γ_f and a new interface with the energy γ_{fs} but removes the old surface with the energy γ_s. Thus the driving force of crystallization is $\Delta\mu = kT(\ln\beta - K_1)$, where $K_1 = \frac{U}{kT} + \frac{(\gamma_f^* - \gamma_s + \gamma_{fs})}{kT}\frac{w}{h}$ and h is the height of the growth step, the superscript * denotes that the stress dependence of the surface energy should be taken into account. Depending on the surface, interface and misfit energies, the value of K_1 can be positive or negative and it can change from one epitaxial layer to another. We cannot calculate the value of K_1 directly, since the values $U < U_{max}$, γ_{fs} and γ_f^* are not known. Moreover, even reliable values of γ_f and γ_s are controversial. The macroscopic precipitation experiments give the values of $\gamma_s = 0.135$ J/m^2 [25] and of $\gamma_s = 0.093$ J/m^2 [26] for barite and of $\gamma_f = 0.120$ J/m^2 for hashemite [25]. From 2D nucleation rates measurements, a value of $\gamma_s = 0.105$ J/m^2 for the (001) barite surface has been determined [21,27]. More recently, Pina et al. [28], on the basis of the classical theory for heterogeneous nucleation derived an expression for calculating crystal face-solution interfacial free energies. Using this method, they determined a value of 0.084 J/m^2. However, for the sake of consistency we take the values provided by Nielsen assuming that the difference $\gamma_f - \gamma_s \approx 0.120 - 0.135 = -0.015$ J/m^2 remains constant. On the other hand the value of K_1 can be estimated from the step velocities and from the nucleation rates.

4.6. Step velocity and nucleation rate

The classical consideration of two-dimensional nucleation provides the following expression for the nucleation rate [29]:

$$J = C\sqrt{\ln\beta}\exp\left(-\frac{\pi h\gamma_f^2 w}{k^2T^2\ln\beta}\right) = C\sqrt{\ln\beta}\exp\left(-\frac{K_2}{\ln\beta}\right), \quad (2)$$

where C is a constant. Application of this expression to heteroepitaxial growth has to consider changes of the driving force caused by elastic and surface/interface contributions. Consequently, Eq. (2) should be rewritten as

$$J = C\sqrt{\ln\beta}\exp\left(-\frac{K_2}{\ln\beta - K_1}\right). \quad (3)$$

Unfortunately, direct application of Eq. (3) is hardly possible, because we do not know the values of C and K_2 and the critical nucleus is not a disk as assumed. The single parameter, which can be estimated is the value of $K_2 = 51.1$. In order to extract some quantitative information, nucleation rates for the first, second and third + fourth layers can be fitted together with given constant value of $K_2 = 51.1$, variable parameter C and independent values of $K_1(i)$ for each layer $i = 1,2,3$. Fig. 3 shows results for the fit with $\ln C = 12$. The values of K_1 were found to be equal to -1.6, -0.5 and -0.95 for the first, second and third + fourth epitaxial layers, respectively. Fitting with another value of K_2 leads to simultaneous increasing or decreasing of $K_1(i)$, so that the differences between these values do not change significantly. Because of the uncertainty in the value of K_2 we can only estimate the differences $K_1(1) - K_1(2) = -1.1$ and $K_1(1) - K_1(3) = -0.65$.

The differences between $K_1(i)$ for the first, second and third + fourth epitaxial layers can be also obtained from step velocities (Fig. 4). Let us assume that the functions V (driving force) for different layers have the same form but are shifted from each other along the abscissa axis on the values $K_1(i) - K_1(j)$. So we can find $K_1(1) - K_1(3) \approx -0.3$ which is not far from the value found from nucleation rates. On the other hand, $K_1(1) - K_1(2) \approx -0.3$ which is significantly lower than the value found from nucleation rates. For the experiment with $\ln\beta = 1.773$, however, growth velocities of the second layer are grouped in two groups—with high and low values. The lower values seem to be more correct, since they were measured at apparently more perfect areas of the crystal surface, where the surface imperfection has a minor contribution in the stress relaxation. From these measurements, we have obtained $K_1(1) - K_1(2) \approx -1.05$ which is very close to values calculated from

nucleation rates. Thus the agreement between K_1 values calculated by different ways was found only for one growth run, the origin of discrepancies for other growth runs remains unclear. In the following discussion we will use the data on the nucleation rates, which seem to be more reliable.

Although the values of $K_1(i)$ depend on three unknown values we can try to compare the experiment and the theory using some simplifications. Let us assume that the first layer has no stress $K_1(1) \approx \frac{(\gamma_f^* - \gamma_s + \gamma_{fs})}{kT} \frac{w}{h}$, the second layer formed on the flat hashemite surface has a maximal value of stress but negligible interface energy $K_1(2) \approx U_{max}/kT$. Finally the third + fourth layers formed on two (three) hashemite layers in substantially imperfect regions are accompanied by lower stress and also by negligible interface energy $K_1(3) \approx U/kT$. As it was shown above $U_{max}/kT = 1.275$, hence, the stress energy in the third + fourth layer is equal to $U \approx 0.65 U_{max}$ and $\gamma_f^* - \gamma_s + \gamma_{fs} \approx 0.003$ J/m^2. The difference $(\gamma_f^* - \gamma_s + \gamma_{fs}) - (\gamma_f - \gamma_s) = \gamma_f^* - \gamma_f + \gamma_{fs} > 0$, but deviation from the zero value is expected to be slight. Substitution of the numerical values gives the plausible value of $\gamma_f^* - \gamma_f + \gamma_{fs} = 0.003 - (-0.015) = 0.018$ J/m^2. Certainly, these estimates are very rough and rather speculative but they look quite reasonable and can confirm the qualitative conclusions outlined above.

5. Conclusions

The nanoscale in situ observations of $BaCrO_4$ on $BaSO_4$ (001) heteroepitaxial growth have shown that the first hashemite layer grows via two-dimensional nucleation and easily forms a complete epitaxial layer, which is likely to have a low level of intrinsic stress. Two-dimensional nucleation of the second and subsequent layers proceeds at significantly lower rates, and is accompanied by lower growth step velocities. These layers seem to have significant level of intrinsic stress and tend to reduce it via formation of free surface normal to the growth layer (holes in layer, dendrite-like shape of nuclei and steps, preferable formation of nuclei at the step edges). As a result the initially flat surface becomes rough. The process described corresponds to the Stranski-Krastanov epitaxial growth mode well known for growth of semiconductors and metals [1–3]. This epitaxial mode is observed in crystal growth from aqueous solutions for the first time.

Acknowledgements

A.G. Shtukenberg acknowledges financial support from the joint Russian-Germany "Mikhail Lomonosov" program (project A/04/38426). J.M. Astilleros acknowledges financial support from Spanish Ministry of Science and Technology ("Ramón y Cajal" program) and the "Consejería de Educación de la Comunidad de Madrid". This work was partially supported by the Spanish Ministry of Science and Technology (Project BTE2002-00325).

References

[1] A. Pimpinelli, J. Villain, Physics of Crystal Growth, Cambridge University Press, Cambridge, 1998.
[2] R. Koch, J. Phys.: Condens. Matter 6 (1994) 9519.
[3] R. Koch, in: D.A. King, D.P. Woodruff (Eds.), Growth and Properties of Ultrathin Epitaxial Layers, Elsevier Science B.V., 1997, p. 448.
[4] J.M. Astilleros, C.M. Pina, L. Fernández-Díaz, A. Putnis, Geochim. Cosmochim. Acta 66 (2002) 3177.
[5] J.M. Astilleros, C.M. Pina, L. Fernández-Díaz, A. Putnis, Surf. Sci. 545 (2003) L773.
[6] P.D. Glynn, E.J. Reardon, Am. J. Sci. 278 (1990) 164.
[7] E.A. Deer, R.A. Howie, J. Zussman, Rock Forming Minerals, vol. 5, Longman, London, 1962.
[8] C.W.F.T. Pistorius, M.C. Pistorius, Z. Kristallogr. 117 (1962) 259.
[9] D.L. Parkhurst, C.A.J. Appelo, User's guide to PHREEQC (version 2) a computer program for speciation, batch-reaction, one-dimensional transport, and inverse geochemical calculations (US Geological Survey. Water Resources Investigation Report 99-4259, 2000), p. 312.
[10] O. Lukkari, H. Lukkari, Suomen Kemistilehti 45B (1972) 6.
[11] C.W. Blount, Am. Mineral. 62 (1977) 942.
[12] C.M. Pina, U. Becker, P. Risthaus, D. Bosbach, A. Putnis, Nature 395 (1998) 483.
[13] C.M. Pina, D. Bosbach, M. Prieto, A. Putnis, J. Cryst. Growth 187 (1998) 119.
[14] R.I. Ristic, B.Yu. Shekunov, J.N. Sherwood, J. Cryst. Growth 179 (1997) 205.
[15] A.A. Chernov, L.N. Rashkovich, A.A. Mkrtchyan, Sov. Phys. Crystallogr. 32 (1987) 432.

[16] L.N. Rashkovich, B.Yu. Shekunov, V.N. Voitsekhovskii, M.V. Shvedova, Sov. Phys. Crystallogr. 34 (1989) 925.
[17] D.J. Srolovitz, Acta Metall. 37 (1989) 621.
[18] B.J. Spencer, P.W. Voorhees, S.H. Davis, J. Appl. Phys. 73 (1993) 4955.
[19] C. Missbach, F. Renard, J.-P. Gratie, K. Kassner, Geophys. Res. Lett. 31 (2004) L06618.
[20] J.M. Astilleros, C.M. Pina, L. Fernández-Díaz, A. Putnis, Chem. Geol. 193 (2003) 93.
[21] P. Risthaus, Rasterkraftmikroskopische Untersuchungen zum Kristallwachstum von Baryt ($BaSO_4$) und isotyper Minerale: Mechanismen und Kinetik im molekularen Maßstab. Doctoral Thesis (Münster, 2003), 119 p.
[22] H. Landolt, R. Börnstein, Elastic, piezoelectric, piezooptic, elastooptic constants and nonlinear dielectric susceptibilities of crystals, New Series, Group III, vol. 18, Springer-Verlag, Berlin, Heidelberg, New York, Tokyo, 1984.
[23] S.V. Moshkin, M.A. Kuz'mina, O.M. Boldyreva, T.I. Ivanova, Crystallogr. Rep. 45 (2000) 1041.
[24] M.A. Kuz'mina, S.V. Moshkin, O.M. Boldyreva, I.P. Shakhverdova, Physics of crystallization, Tver state university, Tver, 1994, p. 103 (in Russian).
[25] A.E. Nielsen, O. Söhnel, J. Cryst. Growth 11 (1971) 233.
[26] S. He, J.E. Oddo, M.B. Tomson, J. Colloid Interf. Sci. 174 (1995) 319.
[27] D. Bosbach, in: R. Hellmann, S.A. Wood (Eds.), Experimental and Environmental Geochemistry: A Tribute to David A. Crerar, Geochemical Society Special Publication 7, The Geochemical Society, St. Louis, 1997, p. 97.
[28] C.M. Pina, A. Putnis, J.M. Astilleros, Chem. Geol. 204 (2004) 145.
[29] M. Ohara, P.C. Reid, Modelling Crystal Growth Rates from Solutions, Prentice Hall, Inc., Englewood Cliffs, NJ, 1973.